



Efficient and Stable Photocatalytic Hydrogen Evolution Activity of Multi-Heterojunction Composite Photocatalysts: CdS and NiS₂ Co-modified NaNbO₃ Nanocubes

Jingjing Xu^{1*}, Jiawei Zhu¹, Junfeng Niu², Mindong Chen¹ and Junpeng Yue¹

¹ Jiangsu Key Laboratory of Atmospheric Environment Monitoring and Pollution Control, Collaborative Innovation Center of Atmospheric Environment and Equipment Technology, Jiangsu Engineering Technology Research Center of Environmental Cleaning Materials, School of Environmental Science and Engineering, Nanjing University of Information Science and Technology, Nanjing, China, ² Research Center for Eco-Environmental Engineering, Dongguan University of Technology, Dongguan, China

OPEN ACCESS

Edited by:

Nelson Marmiroli,
University of Parma, Italy

Reviewed by:

Dong Guohui,
Shaanxi University of Science and
Technology, China
Jingyu Wang,
Huazhong University of Science and
Technology, China

*Correspondence:

Jingjing Xu
xujj@seu.edu.cn; xujj@nuist.edu.cn

Specialty section:

This article was submitted to
Catalysis and Photocatalysis,
a section of the journal
Frontiers in Chemistry

Received: 11 October 2019

Accepted: 06 December 2019

Published: 21 January 2020

Citation:

Xu J, Zhu J, Niu J, Chen M and Yue J
(2020) Efficient and Stable
Photocatalytic Hydrogen Evolution
Activity of Multi-Heterojunction
Composite Photocatalysts: CdS and
NiS₂ Co-modified NaNbO₃
Nanocubes. *Front. Chem.* 7:880.
doi: 10.3389/fchem.2019.00880

In this study, a NaNbO₃/CdS/NiS₂ ternary composite photocatalyst containing no precious metals was successfully prepared by a simple hydrothermal method. The prepared ternary photocatalyst has a significant improvement in photocatalytic performance of hydrogen production from water splitting under visible light irradiation. The best sample NCN40% hydrogen production rate is 4.698 mmol g⁻¹ h⁻¹, which is about 24.7 times that of pure CdS sample. In addition, the stability of the composite catalyst in the long-term photocatalytic hydrogen production cycle is also improved. The reason for the enhanced hydrogen production performance may be the optimization of the microstructure of the catalyst and the reduction of photogenerated electron-hole recombination. The construction of multi-heterojunctions (NaNbO₃-CdS, CdS-NiS₂, and NaNbO₃-NiS₂) helps to reduce the recombination of carriers. Furthermore, the *in-situ*-formed NiS₂ nanoparticles can serve as active sites for hydrogen evolution. All of these factors induced the improved photocatalytic activity of the as-prepared ternary photocatalyst.

Keywords: H₂ evolution, noble-metal-free cocatalyst, NaNbO₃, CdS, NiS₂

INTRODUCTION

Hydrogen is regarded as the clean energy with the greatest development potential in the twenty-first century, with the advantages of high calorific value and no pollution (Esswein and Nocera, 2007; Dempsey et al., 2009; Wang et al., 2018; Mu et al., 2020a). It is a fact that 70% of the earth's surface is water, so many researchers focus on obtaining hydrogen energy through photolysis of water (Hou et al., 2017; Ruan et al., 2018; Yan et al., 2018; Zhang C. et al., 2018; Yu et al., 2019). Many semiconductor-based photocatalysts such as sulfides, nitrides, and metal oxides have been synthesized and studied for photocatalytic hydrogen production (Yu et al., 2016; Zhang G. et al., 2017; Wu et al., 2018; Li J. et al., 2019; She et al., 2019). However, the performance of these photocatalysts is still unsatisfactory, so more new materials need to be developed.

NaNbO_3 is a photocatalyst with a typical perovskite structure and also has excellent chemical stability, ionic conductivity, and photocatalytic properties (Li et al., 2009; Kim et al., 2013; Liu et al., 2017; Sun et al., 2017; Zhang B. et al., 2017; Chen et al., 2018). Although, NaNbO_3 has the advantages of redox ability due to large band gap, it also has disadvantages like low charge separation efficiency and low photocatalytic activity (Xu et al., 2015). There have been many reports that NaNbO_3 was combined with C_3N_4 , Bi_2O_3 , CeO_2 , etc. to ameliorate optical performance and limit recombination of charge carriers (Shi et al., 2009; Chen et al., 2014; Qian et al., 2018; Qiao et al., 2019; Singh Vig et al., 2019; Yang F. et al., 2019).

Cadmium sulfide has been studied a lot, which is attributed to the suitable forbidden band width and conduction band position (Cao et al., 2013; Lang et al., 2016; Li et al., 2017; Ma et al., 2017). Although, the narrower bandwidth has higher spectral utilization efficiency, it also brings the disadvantages of low electron-hole separation efficiency and easy corrosion by light (Li et al., 2011; Zhou et al., 2017; Ruan et al., 2018; Dong et al., 2019; Wang et al., 2019a). Dispersing CdS on other nanomaterials and constructing heterojunctions have been shown to improve the photocatalytic activity and reduce photo-etching (Ke et al., 2019; Xu et al., 2019; Yue et al., 2019). According to the excellent stability of NaNbO_3 and the shortcomings of CdS photocatalyst, dispersing CdS on the surface of NaNbO_3 may be a method to increase photocatalytic activity. Active sites are critical to increasing the yield of water splitting. For example, there have been many reports on the preparation of precious metals cocatalyst-modified photocatalysts that can help in restricting the recombination of electrons and holes (Cao et al., 2015; Huang et al., 2017; Naskar et al., 2017; Zhang Y. et al., 2018; Liu et al., 2019; Yang X. et al., 2019). Precious metals are expensive and have very low reserves, so it is necessary to look for the same highly efficient non-precious metals as a substitute for precious metals (Xu and Xu, 2015; Xing et al., 2017; Kang et al., 2019; Wang et al., 2019b; Chen et al., 2020). It has been reported that a compound of a transition metal Ni was used as a cocatalyst to greatly enhance photocatalytic activity (Chen et al., 2017, 2019; Ma et al., 2017; Digraaskar et al., 2019; Li H. et al., 2019; Dong et al., 2020). Therefore, it is possible to introduce NiS_2 into the $\text{NaNbO}_3/\text{CdS}$ system to synthesize ternary composites, further facilitating the separation of charge carries and increasing hydrogen evolution rate.

In this paper, we designed and synthesized a noble-metal-free ternary composite $\text{NaNbO}_3/\text{CdS}/\text{NiS}_2$ (NCN) in which NaNbO_3 was used as a carrier to uniformly disperse CdS and NiS_2 . Multi-heterojunctions (NaNbO_3 -CdS, CdS- NiS_2 , and NaNbO_3 - NiS_2) were constructed and NiS_2 was used as cocatalyst, enriching photogenerated electrons to improve the kinetic of hydrogen evolution. The as-synthesized NCN40% sample had a photocatalytic hydrogen evolution rate of $4.699 \text{ mmol g}^{-1} \text{ h}^{-1}$, which had great improvement compared to pure CdS. NaNbO_3 itself has excellent electrical conductivity and chemical stability. It not only acts as a carrier for CdS to increase the reaction surface with water but also forms a heterojunction with CdS, which can improve light irradiation stability and accelerate charge separation (Al Balushi et al., 2018). As an active site, NiS_2

can improve photocatalytic activity and facilitate the separation of electron-hole pairs.

EXPERIMENTAL

Synthesis of NaNbO_3 Nanocubes and $\text{NaNbO}_3/\text{CdS}/\text{NiS}_2$ Samples

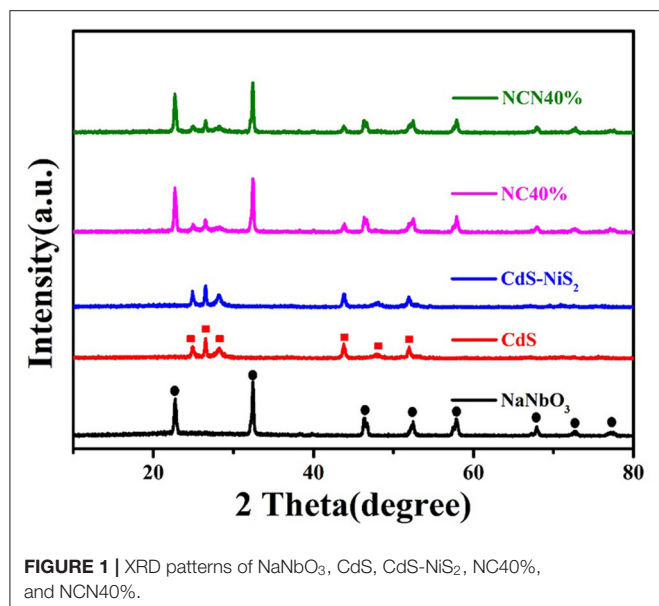
The NaNbO_3 cubes were synthesized by a hydrothermal method (Qian et al., 2018). A total of 2.0 g of Nb_2O_5 was added into sodium hydroxide solution (120 ml, 10 mol/l) and stirred for 120 min. After that, the suspension was heated in a 200-ml Teflon container and kept at 150°C for 48 h. After cooling down, the precipitate was centrifuged and washed with ethanol and pure water for several times until the pH was about 7. Finally, after drying at 60°C , NaNbO_3 nanocubes were obtained.

Synthesis of $\text{NaNbO}_3/\text{CdS}/\text{NiS}_2$ (NCN). As synthesized NaNbO_3 (1.448, 0.7224, and 0.4816 g) was put into pure water (150 ml) and ultrasonically processed for 30 min to disperse entirely. Then, $\text{Cd}(\text{CH}_3\text{COO})_2 \cdot 2\text{H}_2\text{O}$ (2 mmol), $\text{CH}_4\text{N}_2\text{S}$ (4 mmol), and $\text{Ni}(\text{NO}_3)_3 \cdot 6\text{H}_2\text{O}$ (0.2 mmol) were added, and the suspension was stirred for 0.5 h. Afterwards, the suspension was heated at 160°C for 12 h. After cooling, the precipitate was centrifuged, washed with pure water and ethanol, and then dried at 60°C . The obtained samples were tabbed as NCN20%, NCN40%, and NCN60%, and the mass ratios of CdS and NaNbO_3 were 20, 40, and 60%, respectively.

CdS was synthesized as the abovementioned process without addition of NaNbO_3 and $\text{Ni}(\text{NO}_3)_3 \cdot 6\text{H}_2\text{O}$. CdS/NiS_2 and $\text{NaNbO}_3/\text{CdS}$ -40% (NC40%) were also prepared in a similar way. $\text{Cd}(\text{CH}_3\text{COO})_2 \cdot 2\text{H}_2\text{O}$ (2 mmol), $\text{CH}_4\text{N}_2\text{S}$ (4 mmol), and $\text{Ni}(\text{NO}_3)_3 \cdot 6\text{H}_2\text{O}$ (0.2 mmol) were added into pure water and stirred for 0.5 h. Afterwards, the suspension was heated at 160°C for 12 h. After cooling, the precipitate was centrifuged, washed with pure water and ethanol, and then dried at 60°C . The obtained samples were defined as CdS/NiS_2 . For the preparation of $\text{NaNbO}_3/\text{CdS}$ -40% (NC40%), NaNbO_3 (0.7224 g) was added into pure water (150 ml) and ultrasonically treated for 30 min to disperse entirely. Then, $\text{Cd}(\text{CH}_3\text{COO})_2 \cdot 2\text{H}_2\text{O}$ (2 mmol) and $\text{CH}_4\text{N}_2\text{S}$ (4 mmol) were added, and the suspension was stirred for 0.5 h. Afterwards, the suspension was heated at 160°C for 12 h. After cooling, the precipitate was centrifuged and washed with pure water and ethanol before it was dried at 60°C .

Characterizations

The crystal structure and phase characteristics were determined by an X-ray diffractometer at the speed of $10^\circ \text{ min}^{-1}$ with $\text{CuK}\alpha$ radiation (XRD-6100). The chemical composition of the composite sample was determined by multifunctional imaging electron spectrometry (Thermo ESCALAC 250Xi). The microstructure and morphology were obtained by high-resolution projection microscopy (US FEI Tecnai G2 F20). UV-vis DRS spectra was measured on Shimadzu UV3600. PL (Photoluminescence) spectra were researched by Hitachi F-700 fluorescence spectrophotometer. The Brunauer-Emmett-Teller (BET) surface area was obtained by Nitrogen (N_2) adsorption-desorption technique at 77 K on a Quantachrome



IQ-2 instrument. Prior to the measurement of N₂ sorption, the samples were activated at 120°C for about 5 h under vacuum.

The photocurrent response and Mott-Schottky curve were operated on the electrochemical station (Chenhua Instruments, CHI760E), which uses a sample membrane, a platinum plate and Ag/AgCl as electrodes, and 0.5 M Na₂SO₄ as the electrolyte. The sample membrane was a tin fluoride (FTO) conductor glass, which was evenly coated with sample of 1 × 1 cm. The visible light source was a 300-W xenon lamp with a 400-nm filter.

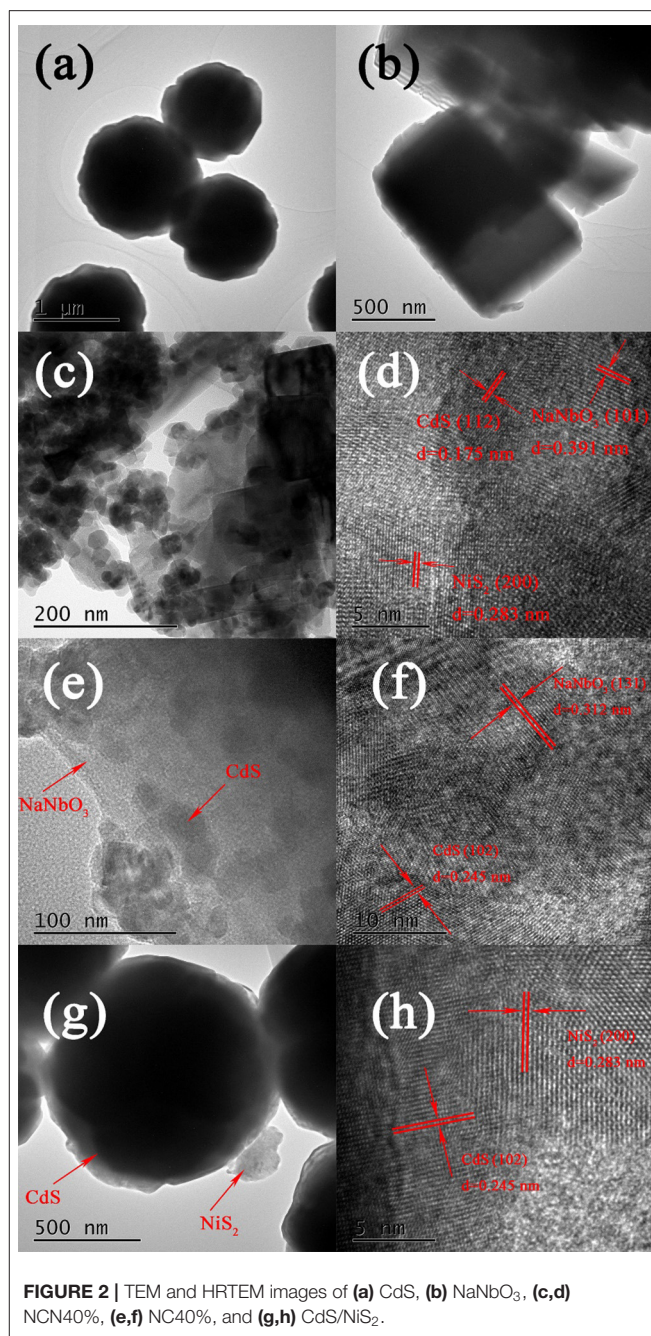
Photocatalytic Hydrogen Evolution Measurement

The photocatalytic H₂ evolution performance was assessed using a photocatalytic activity evaluation system (CEL-SPH2N-D5), followed with gas chromatography (GC-7920) to detect the amount of hydrogen. A total of 25 mg of the photocatalyst, pure water (50 ml), and lactic acid (4 ml) were added into a glass reactor, and the suspension was ultrasonicated and stirred for 5 min for dispersion. After the reactor was connected to the photocatalytic system, continuous pumping took place for more than 20 min to ensure that the entire pipeline was in a vacuum. The visible light source was a 300-W xenon lamp with a 400-nm filter, and room temperature was maintained at 25°C.

RESULTS AND DISCUSSION

Characterization

Figure 1 compares the XRD spectra of the as-synthesized samples to study the crystal phase. Characteristic diffraction peaks at 22.7°, 32.4°, 46.7°, 52.3°, 57.8°, 67.9°, 72.7°, and 77.2° matched with the diffraction peaks of NaNbO₃ (Qian et al., 2018). Characteristic diffraction peaks at 24.8°, 26.5°, 28.2°, 43.7°, 47.8°, and 51.8° matched with the diffraction peaks of CdS (Al Balushi et al., 2018). Characteristic diffraction peaks



of CdS and NaNbO₃ were found in NC40% and NCN40% composites simultaneously, indicating the successful preparation of the target samples. No significant characteristic peaks of NiS₂ were found in the NCN and CdS-NiS₂ composites, probably attributed to low content. Furthermore, there were no impurity peaks.

Figure 2 shows the typical TEM, HRTEM images of NaNbO₃, and CdS NCN40%. As can be seen from **Figures 2a,b**, the clustered circular nanoparticles were pure CdS with a diameter of about 1 μm, and the cube shapes were NaNbO₃ nanocubes. In

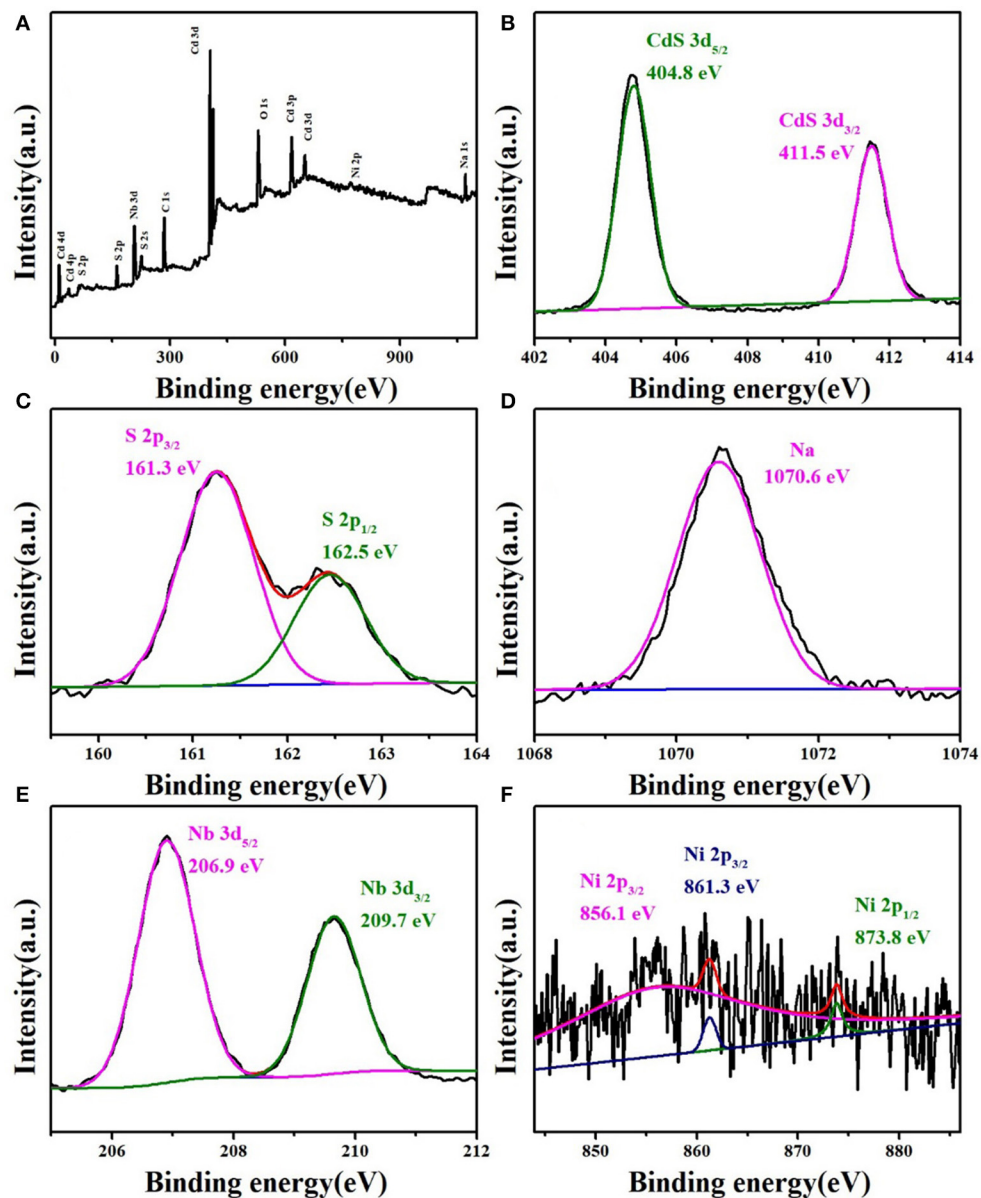


FIGURE 3 | XPS survey spectrum of (A) NCN40%. High-resolution XPS spectra of NCN40%: (B) Cd 3d, (C) S 2p, (D) Na, (E) Nb 3d, and (F) Ni 2p.

HRTEM images (Figure 2c), the spherical and cubic species were CdS, NiS₂, and NaNbO₃, respectively. CdS and NiS₂ particles were grown on the NaNbO₃ cubes uniformly. In Figure 2d, the multi-heterojunctions (NaNbO₃-CdS, CdS-NiS₂, NaNbO₃-NiS₂) were tightly bound, and NiS₂ could be observed. The lattice spacing of 0.175, 0.391, and 0.283 nm were observed corresponding to CdS, NaNbO₃, and NiS₂, respectively (Ma et al., 2017; Al Balushi et al., 2018; Qian et al., 2018). In addition, Figures 2e-h show the microstructure of NC40% and CdS/NiS₂. It can be found that the size of CdS in NaNbO₃/CdS was much smaller than that in CdS/NiS₂. This proved that the existence of NaNbO₃ could greatly reduce the agglomeration of CdS.

Figure 3A shows X-ray photoelectron spectroscopy to confirm the total elemental composition of the NCN40% composite. The Cd, S, Ni, Na, and Nb elements could be found, which further proved the successful preparation of the NCN40% composite sample. The XPS spectra of the elements were also analyzed separately. In Figure 3B, there were characteristic peaks at 404.8 and 411.5 eV (Cd 3d_{5/2} and Cd 3d_{3/2}), consistent with past reports (Yu et al., 2015; Ma et al., 2018). S 2p_{3/2} and S 2p_{1/2} were located at 161.3 and 162.5 eV (Figure 3C), corresponding to CdS and NiS₂ (He et al., 2016; Yue et al., 2019). The peak shown at 1,070.6 eV was Na (Figure 3D) (Wang L. et al., 2017). In Figure 3E, the peaks (206.9 and 209.7 eV) could be attributed

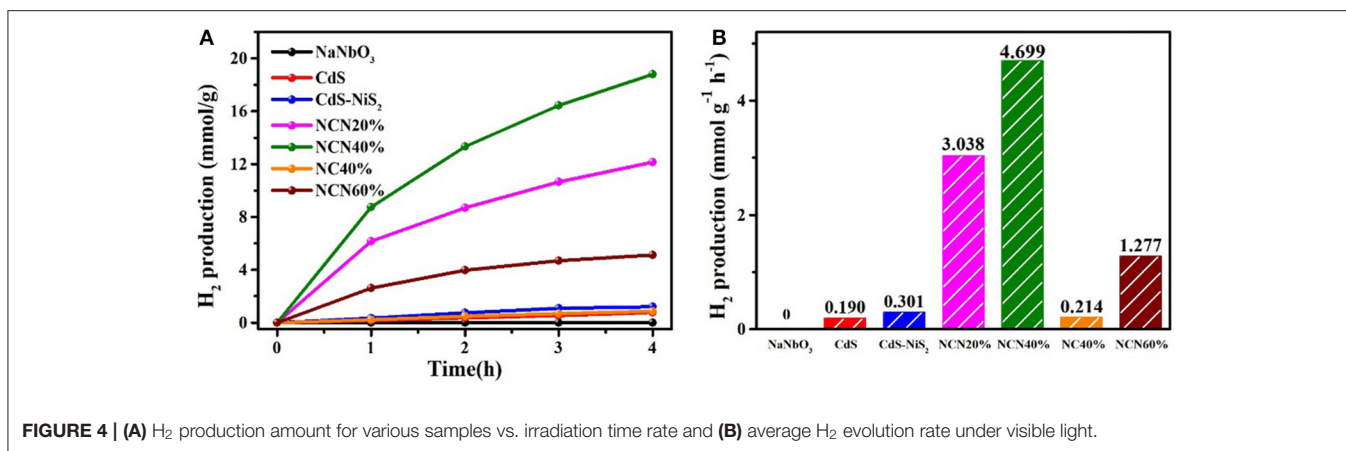


FIGURE 4 | (A) H₂ production amount for various samples vs. irradiation time rate and **(B)** average H₂ evolution rate under visible light.

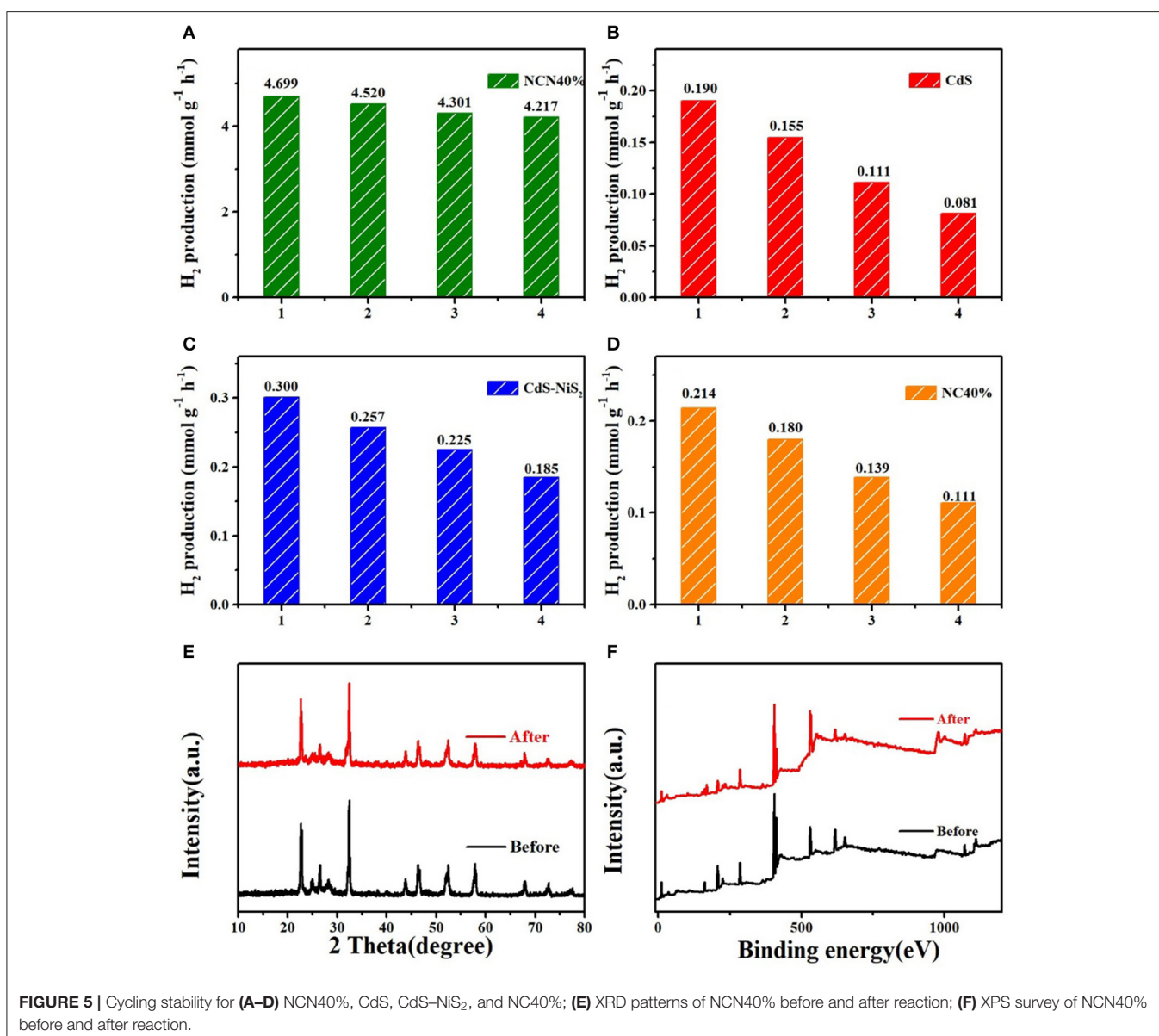
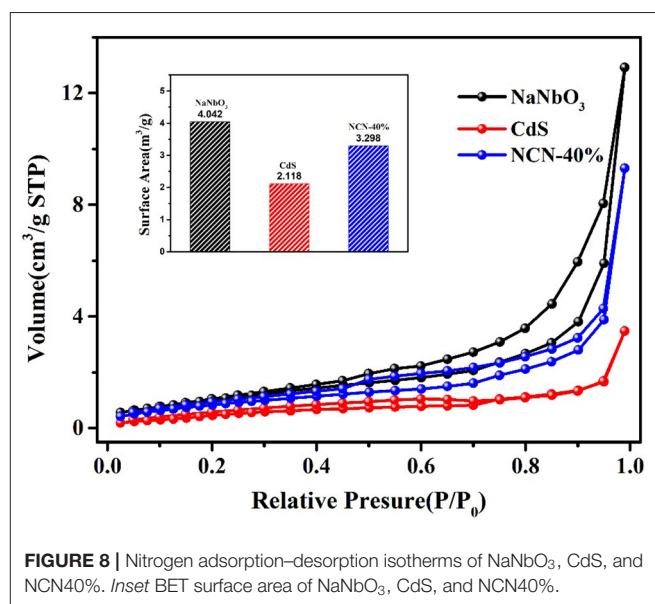
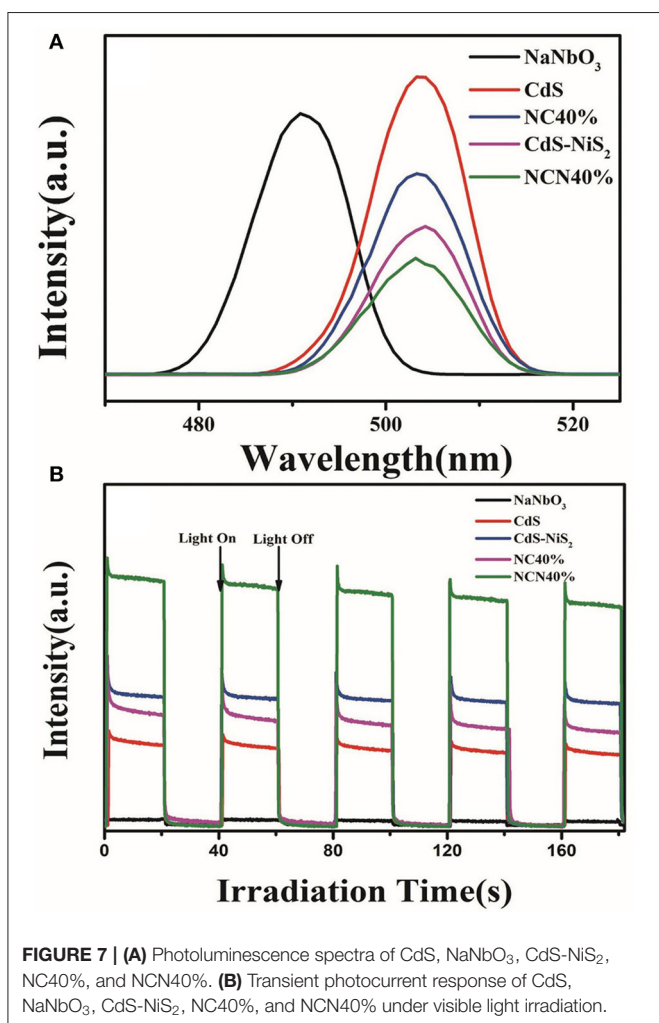
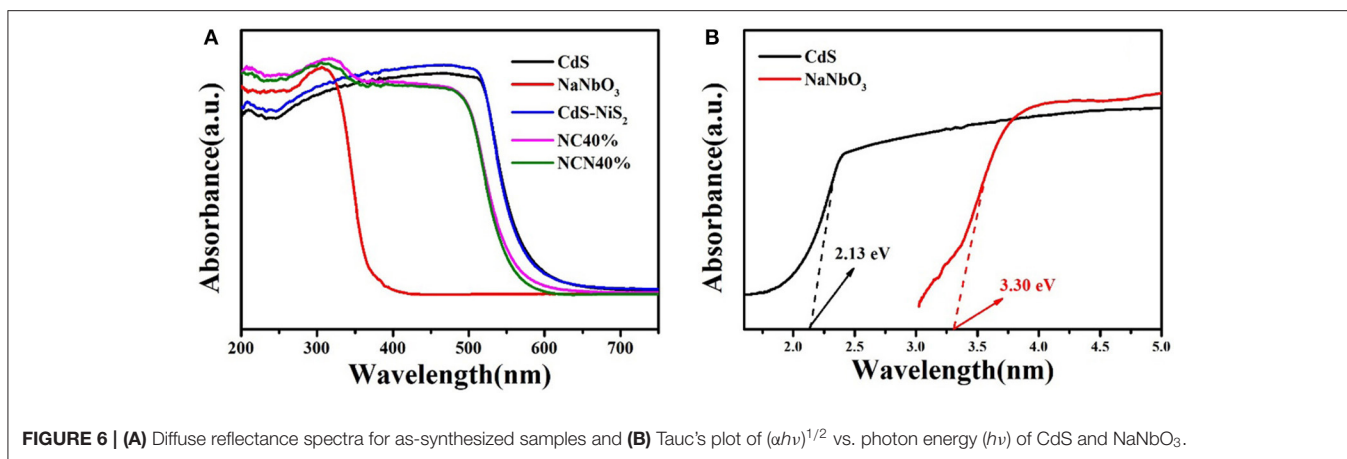


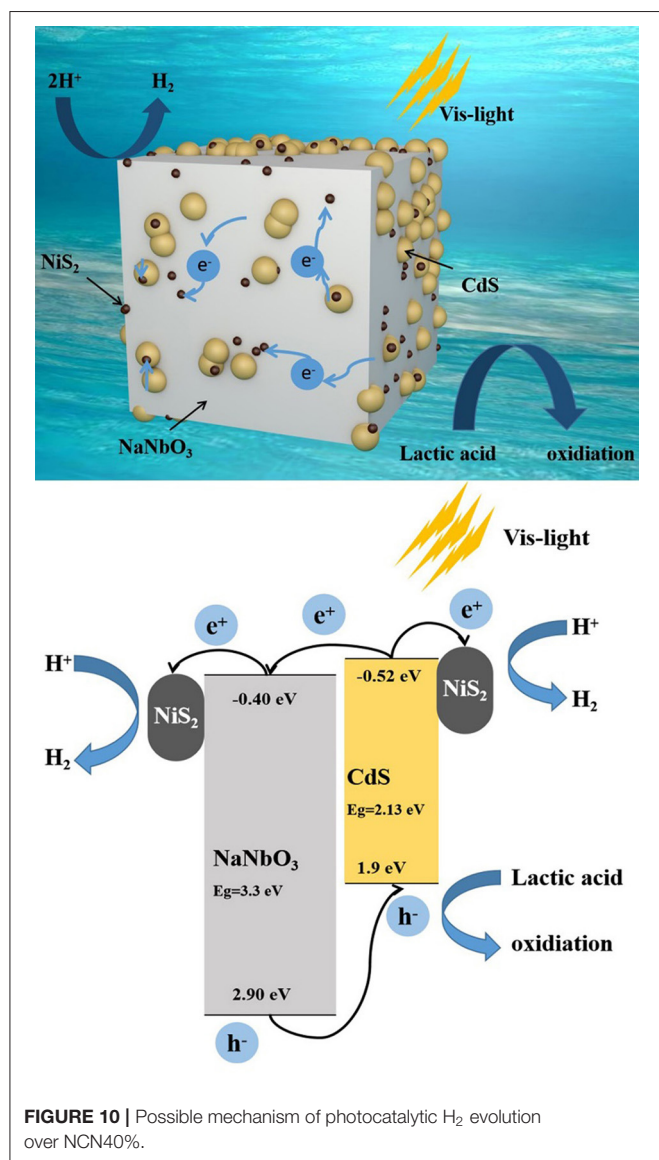
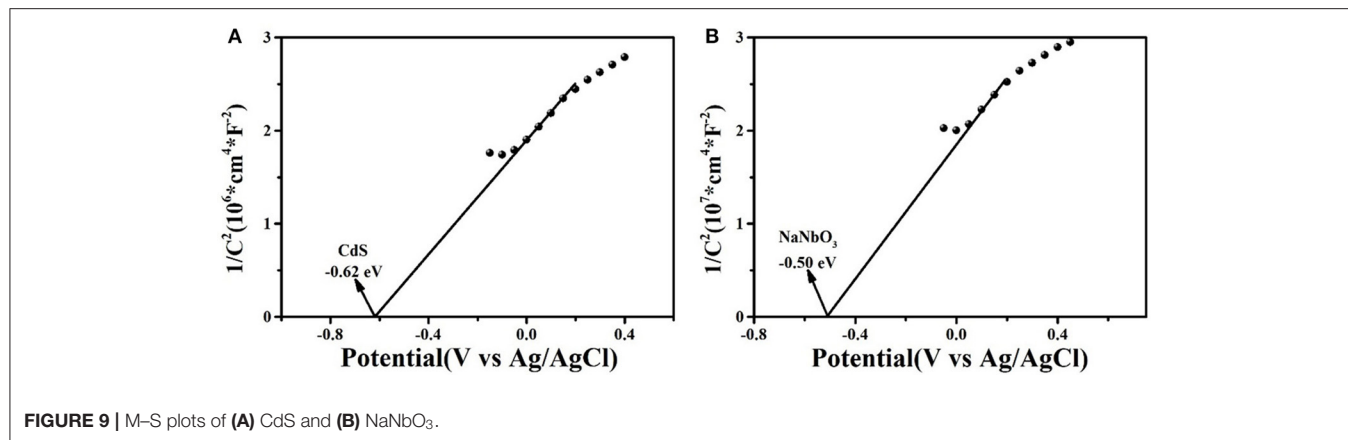
FIGURE 5 | Cycling stability for **(A–D)** NCN40%, CdS, CdS-NiS₂, and NC40%; **(E)** XRD patterns of NCN40% before and after reaction; **(F)** XPS survey of NCN40% before and after reaction.



Photocatalytic H₂ Production and Mechanism

Exposed to visible light irradiation, the hydrogen production rates of NCN samples with different NaNbO₃ contents and CdS, NC40%, and CdS-NiS₂ were studied (Figures 4A,B). Probably because of a large band gap, pure NaNbO₃ showed no response to visible light. CdS was responsive to visible light, but H₂ production efficiency was extremely low (0.190 mmol g⁻¹ h⁻¹), which may be attributed to the instant reunion of electron-hole pairs. After combining with NiS₂, the CdS-NiS₂ sample featured extremely little enhanced hydrogen generation rate (0.301 mmol g⁻¹ h⁻¹). However, the simultaneous combination with NaNbO₃ and NiS₂ greatly boosted the H₂ evolution activity. Especially, the efficiency of NCN40% composite sample was 4.699 mmol g⁻¹ h⁻¹, about 24.7 and 21.9 times that of pure CdS and NC40%, respectively. If the content of NaNbO₃ in the composite sample was low, the CdS particles may not be well-dispersed,

to Nb 3d_{5/2} and Nb 3d_{3/2} (Chen et al., 2014). Figure 3F shows two peaks of Ni 2p_{1/2} and Ni 2p_{3/2} at 856.1 and 873.8 eV (Li H. et al., 2019), and the satellite peak of Ni 2p_{3/2} at 861.3 eV (Ma et al., 2017). XPS spectroscopy further proved the successful preparation of the composite sample.



and too much NaNbO₃ may cause light shielding. It indicated that both NaNbO₃ and NiS₂ had a great effect on improving photocatalytic efficiency.

At the same conditions, four repeated hydrogen production experiments, each lasting for 4 h, were carried out to evaluate the stability of the abovementioned samples. **Figure 5A** showed that the NCN40% maintained high hydrogen production efficiency compared to the first cycle, with about 10.3% reduction. Meanwhile, after four repeated tests, the hydrogen evolution efficiency of CdS, CdS-NiS₂, and CdS-NaNbO₃ was reduced by 57.4, 38.0, and 48.1%, respectively (**Figures 5B–D**). In addition, after repeated tests, there was almost no change in the XRD and XPS (**Figures 5E,F**) spectra of the NCN40% sample compared to the original sample, indicating that the NCN 40% composite had excellent stability under visible light irradiation.

DRS patterns (**Figure 6**) were determined to study the optical properties. Pure NaNbO₃ and pure CdS showed obvious absorption edge at about 350 and 530 nm, conforming to previous reports, respectively (Xu et al., 2011; Wang Q. et al., 2017). The composite of NiS₂ had little effect in CdS/NiS₂ sample. The absorption of the NC40% and NCN40% samples in the ultraviolet region was enhanced, and the light absorption edge was also moved to approximately 500 nm. According to the Kubelka–Munk method: $(\alpha hv)^{1/2} = hv - E_g$ (Ren et al., 2019; Mu et al., 2020b), the band gap energy (E_g) of NaNbO₃ and CdS was 3.30 and 2.13 eV, respectively.

The photoluminescence test further evaluated the recombination efficiency of electrons and holes. The excitation wavelength was set at 340 nm (Kumar et al., 2014). As shown in **Figure 7A**, the photoelectrons and holes in the pure CdS were easily recombined, so that the PL emission spectrum was the highest. When CdS was combined with NiS₂ or NaNbO₃, the intensity of PL emission spectrum was weakened, indicating that the reunion of charge carriers was suppressed.

Transient photocurrent response was operated and analyzed so as to further study the migration and separation efficiency of charge carriers. In **Figure 7B**, NaNbO₃ had almost no photocurrent because it cannot absorb visible light. Then,

it was followed by CdS, NC-40%, and CdS-NiS₂, while the NCN40% composite showed the highest photocurrent intensity. It was consistent with the efficiency of H₂ evolution rate mentioned above. It indicated that the combination of NaNbO₃ or NiS₂ with CdS was beneficial to separate electrons and holes. In NCN composite system, the simultaneous combination of NaNbO₃, NiS₂, and CdS, i.e., multi-heterojunction (NaNbO₃-CdS, CdS-NiS₂, NaNbO₃-NiS₂), was much more significant for the migration efficiency of electrons and holes, meaning that more electrons were used in the hydrogen evolution reaction.

The N₂ adsorption-desorption isotherm was obtained for analysis of the SBET (BET surface area). It could be found in **Figure 8** that the isotherm of NaNbO₃ and CdS was corresponding to type-p and type-n, respectively. The growth of CdS and NiS₂ on NaNbO₃ nanocubes improved the SBET of pure CdS, making more contact area with water and light.

Figure 9 was the Mott-Schottky curves of as-synthesized CdS and NaNbO₃ samples to confirm the conduction band potentials. According to the positive slope (Guohui et al., 2016; Guo et al., 2019; Zhang et al., 2020), CdS and NaNbO₃ were both n-type semiconductors. The flat band potentials of CdS and NaNbO₃ were -0.62 and -0.50 eV, while the normal hydrogen electrode (NHE) could be transformed to -0.52 and -0.40 eV according to equation ($E_{\text{NHE}} = E_{\text{Ag/AgCl}} + 0.1$) (Yue et al., 2019), respectively. Based on the E_{g} measured above, the valence band position of CdS and NaNbO₃ was 1.61 and 2.9 eV, respectively. This staggered energy level position was more favorable for the separation of charges and holes in the heterojunction formed in the composite (Kaowphong et al., 2019).

According to the abovementioned research, the possible mechanism of NaNbO₃/CdS/NiS₂ ternary catalyst to improve hydrogen evolution efficiency is proposed in **Figure 10**. Both CdS and NiS₂ nanoparticles uniformly deposited on NaNbO₃ nanocubes, which greatly reduced the agglomeration of CdS, thus increasing the active sites for hydrogen evolution. CdS responds to visible light, producing electrons and holes. Then, multi-heterojunctions formed by NaNbO₃-CdS, CdS-NiS₂, and NaNbO₃-NiS₂ promote shifting electrons from CdS to NaNbO₃ and NiS₂, while holes left at CdS are consumed by the sacrificial agent. At the same time, NiS₂ in contact with NaNbO₃ or CdS acts as a cocatalyst to further aggregate electrons, providing a number of

stable hydrogen production active sites. In general, the synergistic effect of NaNbO₃ and NiS₂ can accelerate the migration of electrons and holes, in addition to promoting the hydrogen production efficiency of NaNbO₃/CdS/NiS₂ catalytic system.

CONCLUSIONS

In brief, we synthesized noble-metal-free NaNbO₃/CdS/NiS₂ ternary composite by two-step hydrothermal synthesis. Under visible light irradiation, H₂ production rate of ternary catalyst was about 24.7 times that of pure CdS. These may be the possible mechanisms. First, CdS and NiS₂ nanoparticles were uniformly grown on NaNbO₃, which greatly increases the light-receiving area and the reaction area with water, and also improved the repeatability of photocatalytic hydrogen evolution. Second, the simultaneous effect of multi-heterojunction structures and active sites facilitated the migration of photogenerated electrons and holes.

DATA AVAILABILITY STATEMENT

The raw data supporting the conclusions of this manuscript will be made available by the authors, without undue reservation, to any qualified researcher.

AUTHOR CONTRIBUTIONS

JX and MC designed the project, guided the study, and polished the manuscript. JZ conducted the experiments and characterized the samples. JY and JN revised the manuscript.

ACKNOWLEDGMENTS

We are grateful for grants from the Natural Science Foundation of China (51978342), the funding of the Jiangsu Provincial Graduate Research and Innovation Program (SJKY19-0976), Guangdong Innovation Team Project for Colleges and Universities (No. 2016KCXTD023), and Guangdong Province Universities and Colleges Pearl River Scholar Funded Scheme (2017) the Priority Academic Program Development of Jiangsu Higher Education Institutions (PAPD).

REFERENCES

- Al Balushi, B. S. M., Al Marzouqi, F., Al Wahaibi, B., Kuvarega, A. T., Al Kindy, S. M. Z., Kim, Y., et al. (2018). Hydrothermal synthesis of CdS sub-microspheres for photocatalytic degradation of pharmaceuticals. *Appl. Surf. Sci.* 457, 559–565. doi: 10.1016/j.apsusc.2018.06.286
- Cao, M., Wang, P., Ao, Y., Wang, C., Hou, J., and Qian, J. (2015). Investigation on graphene and Pt co-modified CdS nanowires with enhanced photocatalytic hydrogen evolution activity under visible light irradiation. *Dalton Trans.* 44, 16372–16382. doi: 10.1039/c5dt02266e
- Cao, S.-W., Yuan, Y.-P., Fang, J., Shahjamali, M. M., Boey, F. Y. C., Barber, J., et al. (2013). *In-situ* growth of CdS quantum dots on g-C₃N₄ nanosheets for highly efficient photocatalytic hydrogen generation under visible light irradiation. *Int. J. Hydrogen Energy* 38, 1258–1266. doi: 10.1016/j.ijhydene.2012.10.116
- Chen, D., Liu, Z., Guo, Z., Yan, W., and Ruan, M. (2020). Decorating Cu₂O photocathode with noble-metal-free Al and NiS cocatalysts for efficient photoelectrochemical water splitting by light harvesting management and charge separation design. *Chem. Eng. J.* 381:122655. doi: 10.1016/j.cej.2019.122655
- Chen, F., Zhang, L., Wang, X., and Zhang, R. (2017). Noble-metal-free NiO@Ni-ZnO/reduced graphene oxide/CdS heterostructure for efficient photocatalytic hydrogen generation. *Appl. Surf. Sci.* 422, 962–969. doi: 10.1016/j.apsusc.2017.05.214
- Chen, S., Hu, Y., Ji, L., Jiang, X., and Fu, X. (2014). Preparation and characterization of direct Z-scheme photocatalyst Bi₂O₃/NaNbO₃

- and its reaction mechanism. *Appl. Surf. Sci.* 292, 357–366. doi: 10.1016/j.apsusc.2013.11.144
- Chen, W., Hu, Y., and Ba, M. (2018). Surface interaction between cubic phase NaNbO_3 nanoflowers and Ru nanoparticles for enhancing visible-light driven photosensitized photocatalysis. *Appl. Surf. Sci.* 435, 483–493. doi: 10.1016/j.apsusc.2017.11.115
- Chen, Z., Yu, Y., She, X., Xia, K., Mo, Z., Chen, H., et al. (2019). Constructing Schottky junction between 2D semiconductor and metallic nickel phosphide for highly efficient catalytic hydrogen evolution. *Appl. Surf. Sci.* 495:143528. doi: 10.1016/j.apsusc.2019.07.270
- Dempsey, J. L., Brunschwig, B. S., Winkler, J. R., and Gray, H. B. (2009). Hydrogen evolution catalyzed by cobaloximes. *Acc. Chem. Res.* 42, 1995–2004. doi: 10.1021/ar900253e
- Digraskar, R. V., Mali, S. M., Tayade, S. B., Ghule, A. V., and Sathe, B. R. (2019). Overall noble metal free Ni and Fe doped $\text{Cu}_2\text{ZnSnS}_4$ (CZTS) bifunctional electrocatalytic systems for enhanced water splitting reactions. *Int. J. Hydrogen Energy* 44, 8144–8155. doi: 10.1016/j.ijhydene.2019.02.054
- Dong, G., Zhao, L., Wu, X., Zhu, M., and Wang, F. (2019). Photocatalysis removing of NO based on modified carbon nitride: the effect of celestite mineral particles. *Appl. Catal. B Environ.* 245, 459–468. doi: 10.1016/j.apcatb.2019.01.013
- Dong, H., Meng, X.-B., Zhang, X., Tang, H.-L., Liu, J.-W., Wang, J.-H., et al. (2020). Boosting visible-light hydrogen evolution of covalent-organic frameworks by introducing Ni-based noble metal-free co-catalyst. *Chem. Eng. J.* 379:122342. doi: 10.1016/j.cej.2019.122342
- Esswein, A. J., and Nocera, D. G. (2007). Hydrogen production by molecular photocatalysis. *Chem. Rev.* 107, 4022–4047. doi: 10.1021/cr050193e
- Guo, Y., Ao, Y., Wang, P., and Wang, C. (2019). Mediator-free direct dual-Z-scheme $\text{Bi}_2\text{S}_3/\text{BiVO}_4/\text{MgIn}_2\text{S}_4$ composite photocatalysts with enhanced visible-light-driven performance towards carbamazepine degradation. *Appl. Catal. B Environ.* 254, 479–490. doi: 10.1016/j.apcatb.2019.04.031
- Guohui, D., Liping, Y., Fu, W., Ling, Z., and Chuanyi, W. (2016). Removal of nitric oxide through visible light photocatalysis by g- C_3N_4 modified with perylene imides. *ACS Catal.* 6, 6511–6519. doi: 10.1021/acscatal.6b01657
- He, J., Chen, L., Yi, Z.-Q., Au, C.-T., and Yin, S.-F. (2016). CdS nanorods coupled with WS_2 nanosheets for enhanced photocatalytic hydrogen evolution activity. *Ind. Eng. Chem. Res.* 55, 8327–8333. doi: 10.1021/acs.iecr.6b01511
- Hou, H.-J., Zhang, X.-H., Huang, D.-K., Ding, X., Wang, S.-Y., Yang, X.-L., et al. (2017). Conjugated microporous poly(benzothiadiazole)/ TiO_2 heterojunction for visible-light-driven H_2 production and pollutant removal. *Appl. Catal. B Environ.* 203, 563–571. doi: 10.1016/j.apcatb.2016.10.059
- Huang, H., Tu, S., Zeng, C., Zhang, T., Reshak, A. H., and Zhang, Y. (2017). Macroscopic polarization enhancement promoting photo- and piezoelectric-induced charge separation and molecular oxygen activation. *Angew. Chem. Int. Ed.* 56, 11860–11864. doi: 10.1002/anie.201706549
- Kang, W., Guo, H., and Varma, A. (2019). Noble-metal-free NiCu/CeO_2 catalysts for H_2 generation from hydrous hydrazine. *Appl. Catal. B Environ.* 249, 54–62. doi: 10.1016/j.apcatb.2019.02.066
- Kaowphong, S., Choklap, W., Chachvalutikul, A., and Chandet, N. (2019). A novel $\text{CuInS}_2/\text{m-BiVO}_4$ p-n heterojunction photocatalyst with enhanced visible-light photocatalytic activity. *Colloids Surf. A Physicochem. Eng. Aspects* 579:123639. doi: 10.1016/j.colsurfa.2019.123639
- Ke, X., Dai, K., Zhu, G., Zhang, J., and Liang, C. (2019). In situ photochemical synthesis noble-metal-free NiS on CdS-diethylenetriamine nanosheets for boosting photocatalytic H_2 production activity. *Appl. Surf. Sci.* 481, 669–677. doi: 10.1016/j.apsusc.2019.03.171
- Kim, S., Lee, J.-H., Lee, J., Kim, S.-W., Kim, M. H., Park, S., et al. (2013). Synthesis of monoclinic potassium niobate nanowires that are stable at room temperature. *J. Am. Chem. Soc.* 135, 6–9. doi: 10.1021/ja308209m
- Kumar, S., Khanchandani, S., Thirumal, M., and Ganguli, A. K. (2014). Achieving enhanced visible-light-driven photocatalysis using type-II $\text{NaNbO}_3/\text{CdS}$ core/shell heterostructures. *ACS Appl. Mater. Interfaces* 6, 13221–13233. doi: 10.1021/am503055n
- Lang, D., Cheng, F., and Xiang, Q. (2016). Enhancement of photocatalytic H_2 production activity of CdS nanorods by cobalt-based cocatalyst modification. *Catal. Sci. Technol.* 6, 6207–6216. doi: 10.1039/C6CY00753H
- Li, G., Yang, N., Wang, W., and Zhang, W. F. (2009). Synthesis, Photophysical and photocatalytic properties of N-doped sodium niobate sensitized by carbon nitride. *J. Phys. Chem. C* 113, 14829–14833. doi: 10.1021/jp905559m
- Li, H., Wang, M., Wei, Y., and Long, F. (2019). Noble metal-free NiS_2 with rich active sites loaded g- C_3N_4 for highly efficient photocatalytic H_2 evolution under visible light irradiation. *J. Colloid Interface Sci.* 534, 343–349. doi: 10.1016/j.jcis.2018.09.041
- Li, J., Tang, Y., Jin, R., Meng, Q., Chen, Y., Long, X., et al. (2019). Ultrasonic-microwave assisted synthesis of GO/g- C_3N_4 composites for efficient photocatalytic H_2 evolution. *Solid State Sciences.* 97:105990. doi: 10.1016/j.solidstatesciences.2019.105990
- Li, Q., Guo, B., Yu, J., Ran, J., Zhang, B., Yan, H., et al. (2011). Highly efficient visible-light-driven photocatalytic hydrogen production of CdS-cluster-decorated graphene nanosheets. *J. Am. Chem. Soc.* 133, 10878–10884. doi: 10.1021/ja2025454
- Li, Z., Chen, X., Shangguan, W., Su, Y., Liu, Y., Dong, X., et al. (2017). Prickly Ni_3S_2 nanowires modified CdS nanoparticles for highly enhanced visible-light photocatalytic H_2 production. *Int. J. Hydrogen Energy* 42, 6618–6626. doi: 10.1016/j.ijhydene.2016.12.047
- Liu, Q., Chai, Y., Zhang, L., Ren, J., and Dai, W.-L. (2017). Highly efficient Pt/ NaNbO_3 nanowire photocatalyst: its morphology effect and application in water purification and H_2 production. *Appl. Catal. B Environ.* 205, 505–513. doi: 10.1016/j.apcatb.2016.12.065
- Liu, X., Lai, H., Li, J., Peng, G., Yi, Z., Zeng, R., et al. (2019). Polyaniline sensitized Pt/ TiO_2 for visible-light-driven H_2 generation. *Int. J. Hydrogen Energy* 44, 4698–4706. doi: 10.1016/j.ijhydene.2018.12.094
- Ma, S., Deng, Y., Xie, J., He, K., Liu, W., Chen, X., et al. (2018). Noble-metal-free Ni_3C cocatalysts decorated CdS nanosheets for high-efficiency visible-light-driven photocatalytic H_2 evolution. *Appl. Catal. B Environ.* 227, 218–228. doi: 10.1016/j.apcatb.2018.01.031
- Ma, S., Xu, X., Xie, J., and Li, X. (2017). Improved visible-light photocatalytic H_2 generation over CdS nanosheets decorated by NiS_2 and metallic carbon black as dual earth-abundant cocatalysts. *Chin. J. Catal.* 38, 1970–1980. doi: 10.1016/S1872-2067(17)62965-6
- Mu, R., Ao, Y., Wu, T., Wang, C., and Wang, P. (2020a). Synergistic effect of molybdenum nitride nanoparticles and nitrogen-doped carbon on enhanced photocatalytic hydrogen evolution performance of CdS nanorods. *J. Alloys Compd.* 812:151990. doi: 10.1016/j.jallcom.2019.151990
- Mu, R., Ao, Y., Wu, T., Wang, C., and Wang, P. (2020b). Synthesis of novel ternary heterogeneous anatase- TiO_2 (B) biphasic nanowires/ $\text{Bi}_4\text{O}_5\text{I}_2$ composite photocatalysts for the highly efficient degradation of acetaminophen under visible light irradiation. *J. Hazard. Mater.* 382:121083. doi: 10.1016/j.jhazmat.2019.121083
- Naskar, S., Lübkemann, F., Hamid, S., Freytag, A., Wolf, A., Koch, J., et al. (2017). Synthesis of ternary and quaternary Au and Pt decorated CdSe/CdS heteronano-platelets with controllable morphology. *Adv. Funct. Mater.* 27:1604685. doi: 10.1002/adfm.201604685
- Qian, J., Xue, Y., Ao, Y., Wang, P., and Wang, C. (2018). Hydrothermal synthesis of $\text{CeO}_2/\text{NaNbO}_3$ composites with enhanced photocatalytic performance. *Chin. J. Catal.* 39, 682–692. doi: 10.1016/S1872-2067(17)62975-9
- Qiao, Y., Meng, X., and Zhang, Z. (2019). A new insight into the enhanced visible light-induced photocatalytic activity of $\text{NaNbO}_3/\text{Bi}_2\text{WO}_6$ type-II heterostructure photocatalysts. *Appl. Surf. Sci.* 470, 645–657. doi: 10.1016/j.apsusc.2018.11.048
- Ren, M., Ao, Y., Wang, P., and Wang, C. (2019). Construction of silver/graphitic- C_3N_4 /bismuth tantalate Z-scheme photocatalyst with enhanced visible-light-driven performance for sulfamethoxazole degradation. *Chem. Eng. J.* 378:122122. doi: 10.1016/j.cej.2019.122122
- Ruan, D., Kim, S., Fujitsuka, M., and Majima, T. (2018). Defects rich g- C_3N_4 with mesoporous structure for efficient photocatalytic H_2 production under visible light irradiation. *Appl. Catal. B Environ.* 238, 638–646. doi: 10.1016/j.apcatb.2018.07.028
- She, X., Xu, H., Li, L., Mo, Z., Zhu, X., Yu, Y., et al. (2019). Steering charge transfer for boosting photocatalytic H_2 evolution: integration of two-dimensional semiconductor superiorities and noble-metal-free Schottky junction effect. *Appl. Catal. B Environ.* 245, 477–485. doi: 10.1016/j.apcatb.2018.12.011
- Shi, H., Li, X., Iwai, H., Zou, Z., and Ye, J. (2009). 2-Propanol photodegradation under nitrogen-doped NaNbO_3 powders under visible-light irradiation. *J. Phys. Chem. Solids* 70, 931–935. doi: 10.1016/j.jpcs.2009.05.002

- Singh Vig, A., Rani, N., Gupta, A., and Pandey, O. P. (2019). Influence of Ca-doped NaNbO_3 and its heterojunction with g- C_3N_4 on the photoredox performance. *Solar Energy* 185, 469–479. doi: 10.1016/j.solener.2019.04.088
- Sun, M., Yan, Q., Shao, Y., Wang, C., Yan, T., Ji, P., et al. (2017). Facile fabrication of BiOI decorated NaNbO_3 cubes: a p-n junction photocatalyst with improved visible-light activity. *Appl. Surf. Sci.* 416, 288–295. doi: 10.1016/j.apsusc.2017.04.136
- Wang, J., Chen, J., Wang, P., Hou, J., Wang, C., and Ao, Y. (2018). Robust photocatalytic hydrogen evolution over amorphous ruthenium phosphide quantum dots modified g- C_3N_4 nanosheet. *Appl. Catal. B Environ.* 239, 578–585. doi: 10.1016/j.apcatb.2018.08.048
- Wang, L., Gu, H., He, J., Zhao, T., Zhang, X., Xiao, C., et al. (2017). Scale synthesized cubic NaNbO_3 nanoparticles with recoverable adsorption and photodegradation for prompt removal of methylene blue. *J. Alloys Compd.* 695, 599–606. doi: 10.1016/j.jallcom.2016.10.327
- Wang, P., Wu, T., Ao, Y., and Wang, C. (2019a). Fabrication of noble-metal-free CdS nanorods-carbon layer-cobalt phosphide multiple heterojunctions for efficient and robust photocatalyst hydrogen evolution under visible light irradiation. *Renew. Energy* 131, 180–186. doi: 10.1016/j.renene.2018.07.028
- Wang, P., Xu, S., Chen, F., and Yu, H. (2019b). Ni nanoparticles as electron-transfer mediators and NiSx as interfacial active sites for coordinative enhancement of H_2 -evolution performance of TiO_2 . *Chin. J. Catal.* 40, 343–351. doi: 10.1016/S1872-2067(18)63157-2
- Wang, Q., Lian, J., Ma, Q., Zhang, S., He, J., Zhong, J., et al. (2017). Preparation of carbon spheres supported CdS photocatalyst for enhancement its photocatalytic H_2 evolution. *Catal. Today* 281, 662–668. doi: 10.1016/j.cattod.2016.05.013
- Wu, T., Wang, P., Ao, Y., and Wang, C. (2018). Enhanced visible light activated hydrogen evolution activity over cadmium sulfide nanorods by the synergetic effect of a thin carbon layer and noble metal-free nickel phosphide cocatalyst. *J. Colloid Interface Sci.* 525, 107–114. doi: 10.1016/j.jcis.2018.04.068
- Xing, M., Qiu, B., Du, M., Zhu, Q., Wang, L., and Zhang, J. (2017). Spatially separated CdS shells exposed with reduction surfaces for enhancing photocatalytic hydrogen evolution. *Adv. Funct. Mater.* 27:1702624. doi: 10.1002/adfm.201702624
- Xu, D., Yang, S., Jin, Y., Chen, M., Fan, W., Luo, B., et al. (2015). Ag-decorated ATaO_3 (A = K, Na) nanocube plasmonic photocatalysts with enhanced photocatalytic water-splitting properties. *Langmuir* 31, 9694–9699. doi: 10.1021/acs.langmuir.5b01294
- Xu, H., Liu, C., Li, H., Xu, Y., Xia, J., Yin, S., et al. (2011). Synthesis, characterization and photocatalytic activity of $\text{NaNbO}_3/\text{ZnO}$ heterojunction photocatalysts. *J. Alloys Compd.* 509, 9157–9163. doi: 10.1016/j.jallcom.2011.06.100
- Xu, J., Yan, X., Qi, Y., Fu, Y., Wang, C., and Wang, L. (2019). Novel phosphidated MoS_2 nanosheets modified CdS semiconductor for an efficient photocatalytic H_2 evolution. *Chem. Eng. J.* 375:122053. doi: 10.1016/j.cej.2019.122053
- Xu, Y., and Xu, R. (2015). Nickel-based cocatalysts for photocatalytic hydrogen production. *Appl. Surf. Sci.* 351, 779–793. doi: 10.1016/j.apsusc.2015.05.171
- Yan, T., Li, N., Jiang, Z., Guan, W., Qiao, Z., and Huang, B. (2018). Self-sacrificing template synthesis of CdS quantum dots/Cd-Hap composite photocatalysts for excellent H_2 production under visible light. *Int. J. Hydrogen Energy* 43, 20616–20626. doi: 10.1016/j.ijhydene.2018.09.093
- Yang, F., Zhang, Q., Zhang, L., Cao, M., Liu, Q., and Dai, W.-L. (2019). Facile synthesis of highly efficient Pt/N-rGO/N- NaNbO_3 nanorods toward photocatalytic hydrogen production. *Appl. Catal. B Environ.* 257:117901. doi: 10.1016/j.apcatb.2019.117901
- Yang, X., Chen, Z., Zhou, D., Zhao, W., Qian, X., Yang, Q., et al. (2019). Ultra-low Au-Pt co-decorated TiO_2 nanotube arrays: construction and its improved visible-light-induced photocatalytic properties. *Solar Energy Mater. Solar Cells* 201:110065. doi: 10.1016/j.solmat.2019.110065
- Yu, G., Geng, L., Wu, S., Yan, W., and Liu, G. (2015). Highly-efficient cocatalyst-free H_2 -evolution over silica-supported CdS nanoparticle photocatalysts under visible light. *Chem. Commun.* 51, 10676–10679. doi: 10.1039/c5cc02249e
- Yu, H., Huang, X., Wang, P., and Yu, J. (2016). Enhanced photoinduced-stability and photocatalytic activity of CdS by dual amorphous cocatalysts: synergistic effect of Ti(IV)-hole cocatalyst and Ni(II)-electron cocatalyst. *J. Phys. Chem. C.* 120, 3722–3730. doi: 10.1021/acs.jpcc.6b00126
- Yu, H., Huang, Y., Gao, D., Wang, P., and Tang, H. (2019). Improved H_2 -generation performance of Pt/CdS photocatalyst by a dual-function TiO_2 mediator for effective electron transfer and hole blocking. *Ceramics Int.* 45, 9807–9813. doi: 10.1016/j.ceramint.2019.02.018
- Yue, J., Xu, J., Niu, J., and Chen, M. (2019). Synergistic effects of multiple heterojunctions significantly enhance the photocatalytic H_2 evolution rate $\text{CdS}/\text{La}_2\text{Ti}_2\text{O}_7/\text{NiS}_2$ ternary composites. *Int. J. Hydrogen Energy* 44, 19603–19613. doi: 10.1016/j.ijhydene.2019.05.120
- Zhang, B., Zhang, D., Xi, Z., Wang, P., Pu, X., Shao, X., et al. (2017). Synthesis of $\text{Ag}_2\text{O}/\text{NaNbO}_3$ p-n junction photocatalysts with improved visible light photocatalytic activities. *Separat. Purific. Technol.* 178, 130–137. doi: 10.1016/j.seppur.2017.01.031
- Zhang, C., Zhou, Y., Bao, J., Fang, J., Zhao, S., Zhang, Y., et al. (2018). Structure regulation of $\text{ZnS}@g\text{-C}_3\text{N}_4/\text{TiO}_2$ nanospheres for efficient photocatalytic H_2 production under visible-light irradiation. *Chem. Eng. J.* 346, 226–237. doi: 10.1016/j.cej.2018.04.038
- Zhang, G., Zhou, Y., Fan, X., Zou, J., Dong, W., and Xu, X. (2017). Efficient and robust visible light photocatalytic H_2 production based on CdSe quantum dots sensitized titania. *Int. J. Hydrogen Energy* 42, 19877–19884. doi: 10.1016/j.ijhydene.2017.06.153
- Zhang, S., Yi, J., Chen, J., Yin, Z., Tang, T., Wei, W., et al. (2020). Spatially confined Fe_2O_3 in hierarchical $\text{SiO}_2@\text{TiO}_2$ hollow sphere exhibiting superior photocatalytic efficiency for degrading antibiotics. *Chem. Eng. J.* 380:122583. doi: 10.1016/j.cej.2019.122583
- Zhang, Y., Chen, J., Tang, H., Xiao, Y., Qiu, S., Li, S., et al. (2018). Hierarchically-structured $\text{SiO}_2\text{-Ag}/\text{TiO}_2$ hollow spheres with excellent photocatalytic activity and recyclability. *J. Hazard. Mater.* 354, 17–26. doi: 10.1016/j.jhazmat.2018.04.047
- Zhou, X., Sun, H., Zhang, H., and Tu, W. (2017). One-pot hydrothermal synthesis of CdS/NiS photocatalysts for high H_2 evolution from water under visible light. *Int. J. Hydrogen Energy* 42, 11199–11205. doi: 10.1016/j.ijhydene.2017.03.179

Conflict of Interest: The authors declare that the research was conducted in the absence of any commercial or financial relationships that could be construed as a potential conflict of interest.

Copyright © 2020 Xu, Zhu, Niu, Chen and Yue. This is an open-access article distributed under the terms of the Creative Commons Attribution License (CC BY). The use, distribution or reproduction in other forums is permitted, provided the original author(s) and the copyright owner(s) are credited and that the original publication in this journal is cited, in accordance with accepted academic practice. No use, distribution or reproduction is permitted which does not comply with these terms.